RAA 2019 Vol. **19** No. **9**, 132(10pp) doi: 10.1088/1674–4527/19/9/132

http://www.raa-journal.org *http://iopscience.iop.org/raa*

***R**esearch in*
***A**stronomy and*
***A**strophysics*

DmpIRFs and DmpST: DAMPE instrument response functions and science tools for gamma-ray data analysis

Kai-Kai Duan[1,2], Wei Jiang[1,3], Yun-Feng Liang[1], Zhao-Qiang Shen[1,2], Zun-Lei Xu[1], Yi-Zhong Fan[1,3], Fabio Gargano[4], Simone Garrappa[5,6], Dong-Ya Guo[7], Shi-Jun Lei[1], Xiang Li[1], Mario Nicola Mazziotta[4], Maria Fernanda Munoz Salinas[8], Meng Su[1,9], Valerio Vagelli[5,6], Qiang Yuan[1,3], Chuan Yue[1] and Stephan Zimmer[8]

[1] Key Laboratory of Dark Matter and Space Astronomy, Purple Mountain Observatory, Chinese Academy of Sciences, Nanjing 210033, China; *duankk@pmo.ac.cn, liangyf@pmo.ac.cn, xiangli@pmo.ac.cn*
[2] University of Chinese Academy of Sciences, Beijing 100049, China
[3] School of Astronomy and Space Science, University of Science and Technology of China, Hefei 230026, China
[4] Istituto Nazionale di Fisica Nucleare Sezione di Bari, I-70125, Bari, Italy
[5] Istituto Nazionale di Fisica Nucleare Sezione di Perugia, I-06123 Perugia, Italy
[6] Dipartimento di Fisica e Geologia, Università degli Studi di Perugia, I-06123 Perugia, Italy
[7] Institute of High Energy Physics, Chinese Academy of Sciences, Beijing 100049, China
[8] Department of Nuclear and Particle Physics, University of Geneva, CH-1211, Switzerland
[9] Department of Physics and Laboratory for Space Research, University of Hong Kong, Pok Fu Lam, Hong Kong, China

Received 2019 March 28; accepted 2019 April 23

Abstract Observing GeV gamma-rays is an important goal of the DArk Matter Particle Explorer (DAMPE) for indirect dark matter searching and high energy astrophysics. In this work, we present a set of accurate instrument response functions for DAMPE (DmpIRFs) including the effective area, point-spread function and energy dispersion, which are crucial for gamma-ray data analysis based on statistics from simulation data. A dedicated software named DmpST is developed to facilitate the scientific analyses of DAMPE gamma-ray data. Considering the limited number of photons and angular resolution of DAMPE, the maximum likelihood method is adopted in DmpST to better disentangle different source components. The basic mathematics and framework regarding this software are also introduced in this paper.

Key words: gamma rays: general — instrumentation: detectors — methods: statistical

1 INTRODUCTION

DArk Matter Particle Explorer (DAMPE) is a high energy cosmic-ray and gamma-ray observatory (Chang 2014; Chang et al. 2017). It contains four sub-detectors: a Plastic Scintillation Detector (PSD), a Silicon-Tungsten tracKer-converter (STK), a BGO calorimeter (BGO) and a NeUtron Detector (NUD). The PSD that measures the charge of particles also acts as an anti-coincidence detector for gamma-ray observation. The STK measures the trajectories of charged particles, as well as the photons that are converted into e^+e^- pairs. The BGO calorimeter measures the energies of incident particles and is also able to distinguish electrons from hadrons efficiently. The NUD provides an independent measurement and further improvement for the electron/hadron identification. On-orbit calibration has been adopted for DAMPE and it is expected to operate stably during the next few years (Ambrosi et al. 2019; Ma et al. 2018; Ding et al. 2019; Jiang et al. 2019).

Based on the photon selection algorithm described in Xu et al. (2018), valuable gamma-ray data have been accumulated. Further scientific analysis of high-level gamma-ray data, however, requires detailed knowledge about the instrument response functions (IRFs) of DAMPE, i.e., the effective area, point-spread function (PSF) and energy dispersion function. Based on simulation data, we have con-

structed the IRFs for DAMPE gamma-ray observation in the energy range from 1 GeV to 10 TeV and with the incidence angle from 0° to 60°.

Limited by the relatively low statistics of DAMPE gamma-ray data, the chi-squared method is not suitable for this data analysis, and the maximum likelihood method (Mattox et al. 1996) is adopted. Combining the IRFs and model of gamma-ray sources, we can calculate the expected photon number recorded by the detector. The values, and also the uncertainties, of the parameters in the gamma-ray source model can then be estimated by comparing with the real DAMPE observation using the maximum likelihood method.

The data preparation, convolution with the IRFs and parameter inference are realized for DAMPE data analysis using dedicated software named DmpST, which is also developed to facilitate the scientific analysis. In this paper, we introduce both the DAMPE IRFs and DmpST software.

This paper is structured as follows. We first introduce the IRFs of DAMPE in Section 2. The observing time and exposure of DAMPE are then described in Section 3. In Section 4, we highlight the maximum likelihood method for DAMPE gamma-ray data analysis, followed by a description of the code structures in Section 5. We summarize this work in Section 6.

2 INSTRUMENT RESPONSE FUNCTIONS

IRFs are the parameterized representations of the instrument performance. The DAMPE IRFs can be factorized into three parts (Ackermann et al. 2012). The effective area, $A_{\rm eff}(E,\hat{v},s)$, is the product of the geometrical cross-section area, the probability of gamma-ray conversion and the efficiency of photon selection for a gamma-ray with energy E and direction $\hat{v}$ in the detector reference frame. The s denotes the trigger type (see below). The PSF, $P(\hat{v}';E,\hat{v},s)$, and the energy dispersion function $D(E';E,\hat{v},s)$, are the probability distributions of the reconstructed direction $\hat{v}'$ and reconstructed energy E' for a gamma-ray with energy E and direction $\hat{v}$ respectively.

Given the spatial and spectral model of the incident gamma-ray sources, $F(E,\hat{p})$, where $\hat{p}$ refers to the celestial directions of the gamma-ray sources, we can convolve the model with the IRFs to predict the distribution of observed photons

$$\begin{aligned} r(E',\hat{p}',s) = \int\int\int & F(E,\hat{p})A_{\rm eff}(E,\hat{v}(t;\hat{p}),s) \\ & \times P(\hat{v}'(t;\hat{p}');E,\hat{v}(t;\hat{p}),s) \\ & \times D(E';E,\hat{v}(t;\hat{p}),s){\rm d}E{\rm d}\Omega{\rm d}t, \end{aligned} \tag{1}$$

where $\hat{p}'$ is the reconstructed celestial directions of the gamma-rays. The integrals are over the time and energy range of interest and the solid angle in the celestial reference frame.

To evaluate the DAMPE IRFs, we perform `Geant4`-based Monte Carlo detector simulation to generate pseudo-photons for DAMPE (MC data hereafter). We simulate gamma-rays with uniform distribution of incidence direction, that can be used to explore the instrument response across the entire field of view (FoV) of DAMPE. The MC data are generated with an E^{-1} count spectrum uniformly in the logarithm energy, and from a sphere with 6 m^2 cross-sectional area centered on the detector to cover the whole energy range and the whole detector of DAMPE. The directions of the gamma-rays are sampled uniformly in a solid angle with downward-pointing directions, leading to a semi-isotropic incidence flux of the simulated gamma-rays. Here we ignore the back-entering events, because these events would have to traverse a large amount of material and thus presumably lose a lot of energy along the way. Through the same reconstruction and gamma-ray selection algorithm as the on-orbit data, the MC data can describe the response of DAMPE for gamma-ray observation accurately (Xu et al. 2018).

DAMPE uses two sets of trigger directives for physics data: the pre-scaled Low Energy Trigger (LET) and the High Energy Trigger (HET). The pre-scale factors of the LET are different when the detector is at different geographic latitudes (Chang et al. 2017). When the detector is in the low latitude region ($|\phi_{\rm g}| < 20°$), the LET is pre-scaled by a factor of 8; and at the high latitude region ($|\phi_{\rm g}| > 20°$) it is pre-scaled by 64. The IRFs are also divided into two sub-sets, LET IRFs and HET IRFs.

2.1 Effective Area

Effective area is a numerical function varying with energy of a gamma-ray photon and its incidence direction in the instrument reference frame. We binned the MC data according to the event energy, incidence angle and trigger type. The effective area for each bin centered at E_i, θ_j, ϕ_k with trigger type s is

$$A_{\rm eff}(E_i,\theta_j,\phi_k,s) = \frac{N_{i,j,k,s}}{N_{{\rm sim},i,j,k}} A_{\rm sim}\,, \tag{2}$$

where $N_{{\rm sim},i,j,k}$ is the number of photons generated in the simulation in each bin, and $N_{i,j,k,s}$ is the number of photons that pass the selection algorithm with trigger type s = LET or HET. $A_{\rm sim}$ is the cross-sectional area of the generated sphere in the simulation.

We divide the MC data into 20 energy bins from 1 GeV to 100 GeV (40 energy bins from 1 GeV to 10 TeV) and 10 angular bins from 0° to 60° for LET (HET) data. Figure 1 shows the effective area of DAMPE gamma-ray observations as a function of energy and incidence direction.

2.2 Point-spread Function

The reconstructed direction ($\hat{v}'$) of the photon may deviate from its true value ($\hat{v}$), and the probability distribution of the deviation $\delta v = |\hat{v}' - \hat{v}|$ is parameterized by the PSF. The PSF for DAMPE is related to the inclination angle θ and azimuth angle ϕ of the incident photon in the detector reference frame, and also the photon's energy and trigger type. Because the ϕ dependence of the PSF is much weaker than the θ dependence, we ignore the ϕ dependence in the current version of the PSF.

Based on the MC data, we construct a histogram of angular deviations of the selected gamma-rays for each energy and incidence angle bin and for each trigger type. We find that the form of the *Fermi*-LAT PSF (Ackermann et al. 2012) can accommodate DAMPE simulation data well. Accordingly, the PSF histogram is fitted with a double King function,

$$\begin{aligned} P(x) =& f_{\rm core} K(x_p; \sigma_{\rm core}, \gamma_{\rm core}) \\ &+ (1 - f_{\rm core}) K(x_p; \sigma_{\rm tail}, \gamma_{\rm tail}) \,, \end{aligned} \tag{3}$$

where $K(x_p; \sigma, \gamma)$ is the King function defined as

$$K(x_p; \sigma, \gamma) = \frac{1}{2\pi\sigma^2} \left(1 - \frac{1}{\gamma}\right) \left[1 + \frac{1}{2\gamma} \frac{x_p^2}{\sigma^2}\right]^{-\gamma} , \tag{4}$$

and x_p is the scaled angular deviation

$$x_p = \frac{\delta v}{S_{\rm p}(E, \theta)} \,. \tag{5}$$

The $S_{\rm p}(E, \theta)$ is the angular resolution (defined as 68% containment of the angular deviation) at energy E and incidence angle θ. The functional form of the King profile originates from *XMM-Newton* (Kirsch et al. 2004, Read et al. 2011) and was later adapted for the *Fermi*-LAT. Note that the King function is normalized, i.e., $\int_0^\infty 2\pi x K(x; \sigma, \gamma) {\rm d}x = 1$.

We divide the MC data into four energy bins from 1 GeV to 100 GeV (eight energy bins from 1 GeV to 10 TeV) and five angular bins from 0° to 60° for LET (HET) data. Figure 2 shows the angular resolution of DAMPE for gamma-ray observations at different energies and incidence directions. For each bin, the MC data are fitted with the above functions and their best-fit parameters are derived and stored in DmpST. Figure 3 displays an example of the best fit to the scaled angular deviation with the double King function in the bin of $E \in [3.16, 10]$ GeV and $\theta \in [25.84°, 36.87°]$ for HET photons.

2.3 Energy Dispersion

The energy dispersion function gives the probability of a photon with true energy (E) being allocated an energy (E') after reconstruction of the events. Similar to the PSF, we ignore the ϕ dependence and parameterize the energy dispersion as a function of scaled energy deviation

$$x_D = \frac{E' - E}{S_{\rm D}(E, \theta) E} \,, \tag{6}$$

where the scale $S_{\rm D}(E, \theta)$ is the energy resolution (defined as the half-width of the 68% containment range of the energy deviation) at the bin center of energy E and incidence angle θ. We fit the MC data with three piecewise functions in the form

$$D(x_D) = \begin{cases} N_L R(x_D, x_0, \sigma_L, \gamma_L) & \text{if } (x_D - x_0) < -\bar{x}, \\ N_l R(x_D, x_0, \sigma_l, \gamma_l) & \text{if } (x_D - x_0) \in [-\bar{x}, 0], \\ N_R R(x_D, x_0, \sigma_R, \gamma_R) & \text{if } (x_D - x_0) > 0, \end{cases}$$

$$R(x_D, x_0, \sigma, \gamma) = N \exp\left(-\frac{1}{2} \left| \frac{x_D - x_0}{\sigma} \right|^\gamma \right) . \tag{7}$$

We divided the MC data with the same binned method as the PSF. Figure 4 shows the energy resolution of DAMPE for gamma-ray observation at different energies and incidence directions. We fit the energy dispersion with the above function in each bin. Figure 5 depicts an example of energy dispersion fitted with the function in the bin of $E \in [3.16, 10]$ GeV and $\theta \in [25.84°, 36.87°]$ for HET photons.

3 OBSERVING TIME AND EXPOSURE

For a particular source in the sky, its direction in the detector reference frame varies with time. Since the IRFs vary appreciably across the DAMPE FoV, we define the exposure ϵ for any given energy E and direction in the sky $\hat{p}$ as the integral of the effective area over the time range of interest,

$$\epsilon(E, \hat{p}) = \sum_s \int A_{\rm eff}(E, \hat{v}(t, \hat{p}), s) {\rm d}t \,. \tag{8}$$

The exposure can also be expressed as an integral over the solid angle in the detector reference frame,

$$\begin{aligned} \epsilon(E, \hat{p}) \;&=\; \sum_s \int A_{\rm eff}(E, \hat{v}, s) t_{\rm obs}(\hat{v}; \hat{p}) {\rm d}\Omega \\ &=\; \int A_{\rm eff}^{\rm LET} t_{\rm obs} {\rm d}\Omega + \int A_{\rm eff}^{\rm HET} t_{\rm obs} {\rm d}\Omega \,. \end{aligned} \tag{9}$$

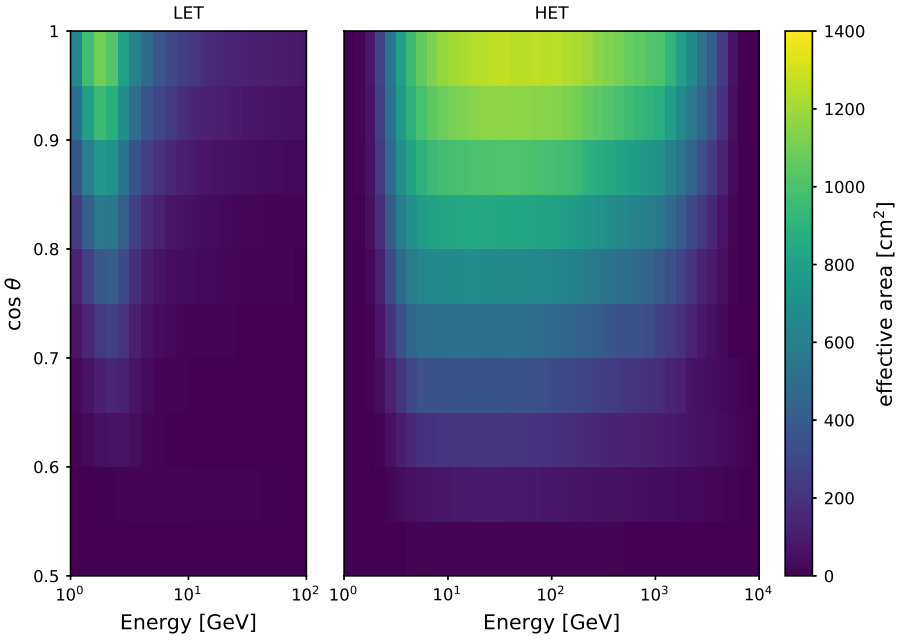

Fig. 1 The effective area of DAMPE (in units of cm^2) for gamma-ray observation at different energies and incidence directions. The energy is in 20 bins from 1 GeV to 100 GeV for LET photons (*left panel*) and 40 bins to 10 TeV for HET photons (*right panel*). The incidence angle is in 10 bins from 0° to 60°. Note that the effective area presented here is averaged over ϕ.

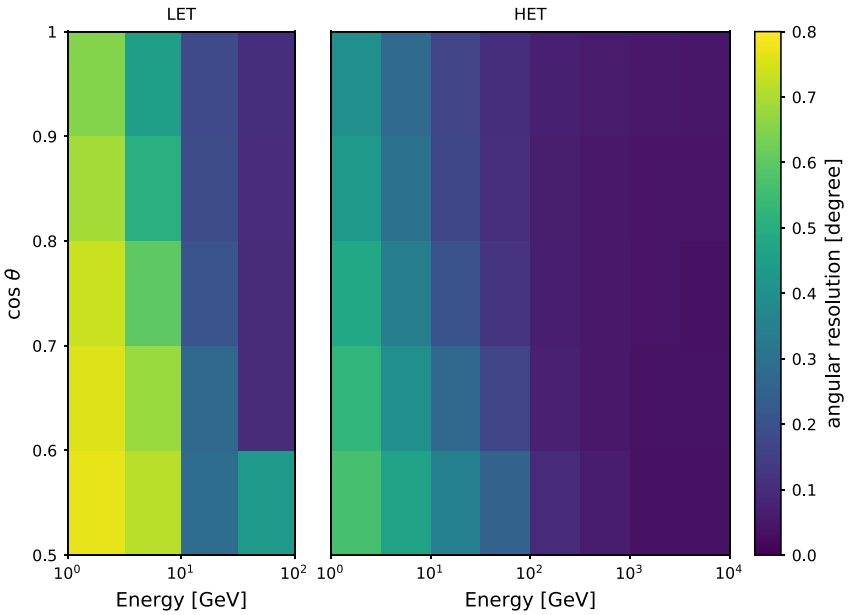

Fig. 2 The angular resolution of DAMPE (in units of degree) for gamma-ray observation at different energies and incidence directions. The energy is in four bins from 1 GeV to 100 GeV for LET photons (*left panel*) and eight bins to 10 TeV for HET photons (*right panel*). The incidence angle is in five bins from 0° to 60°.

Here the $t_{\rm obs}(\hat{v};\hat{p})$ is named *observing time* and defined as the total time in the range of interest during which DAMPE has observed the direction $\hat{p}$ with detector frame direction $\hat{v}$. $A_{\rm eff}^{\rm LET}$ and $A_{\rm eff}^{\rm HET}$ in Equation (9) are the effective area for LET and HET photons, respectively. As an example, we show the observing time map in the detector reference frame for the Vela pulsar in Figure 6. With the observing time map and the DAMPE effective area, the exposure then can be calculated according to Equation (9). Figure 7 displays the all-sky exposure map of DAMPE at 10 GeV for

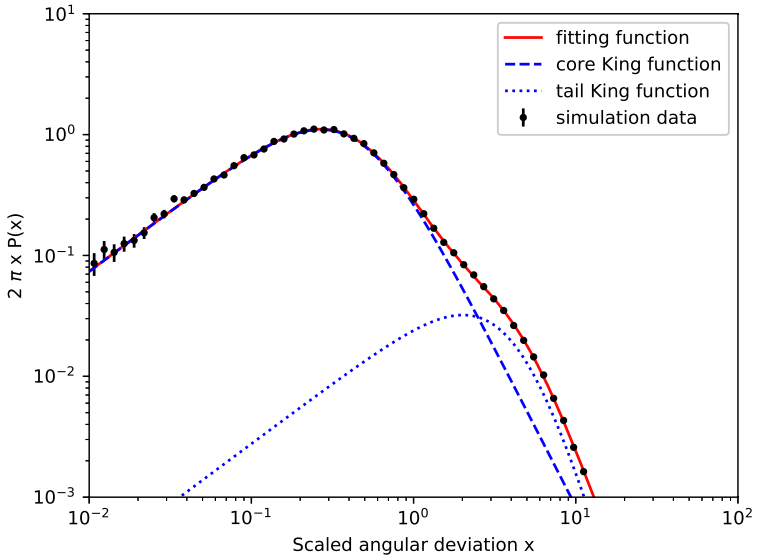

Fig. 3 The best fit to the scaled angular deviation with double King function in the energy range [3.16, 10] GeV and incidence angle range [25.84°, 36.87°] for HET photons. The *points* are the distribution of the scaled angular deviation for the MC data, the *dashed* and *dotted lines* are the core and tail King functions respectively and the *solid line* is the sum of the two components. The reduced χ^2 of this fitting is 1.09.

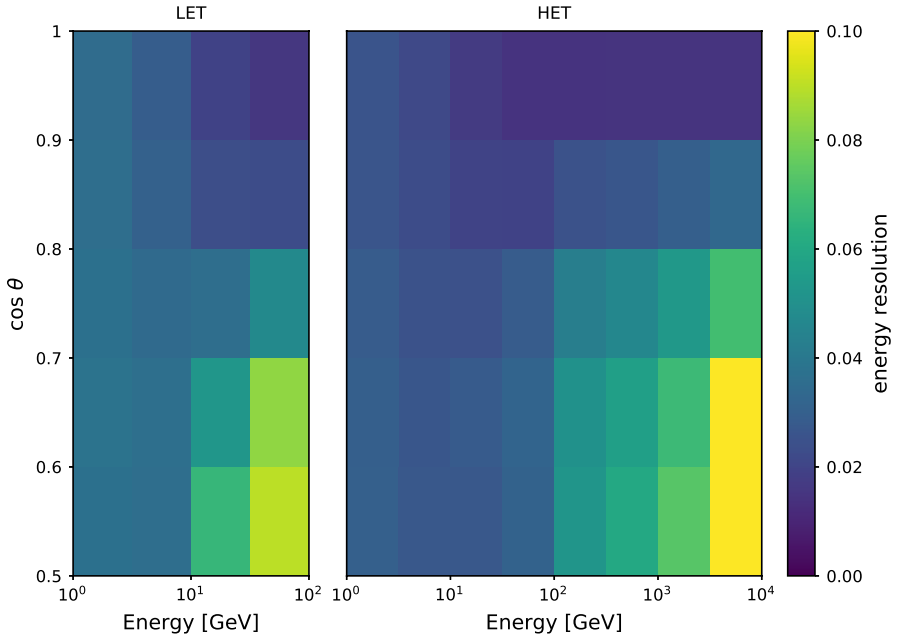

Fig. 4 The energy resolution of DAMPE (dimensionless) for gamma-ray observation at different energies and incidence directions. The energy is in four bins from 1 GeV to 100 GeV for LET photons (*left panel*) and eight bins to 10 TeV for HET photons (*right panel*). The incidence angle is in five bins from 0° to 60°.

the first year of operation. Because DAMPE is in a Sun-synchronous orbit, we can see that the exposure is not uniform over the sky.

4 MAXIMUM LIKELIHOOD ANALYSIS

Analyzing the gamma-ray data from DAMPE requires the maximum likelihood method due to the limited number of photons and angular resolution. We characterize a source by its photon flux density $F(E, \hat{p}, t; \boldsymbol{\lambda})$. In order to reduce the computational burden, we assume the source is stationary during the time range in each likelihood analysis. [1] A

[1] For a variable source, time dependence of the flux can be achieved by repeating the analysis in finer time bins.

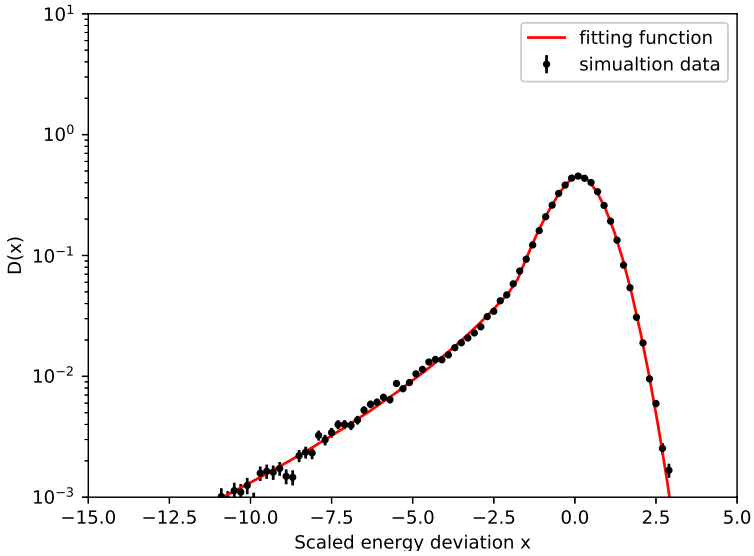

Fig. 5 The best fit to the scaled energy deviation with the energy dispersion function in the energy range [3.16, 10] GeV and incidence angle range [25.84°, 36.87°] for HET events. The *points* are the scaled deviation distribution of the MC data, and the *line* is the best fit function. The reduced χ^2 of this fitting is 1.05.

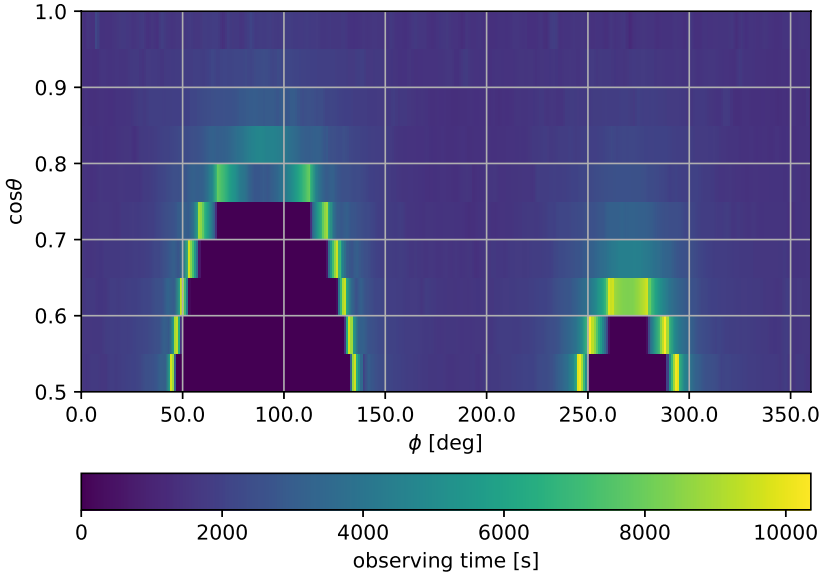

Fig. 6 The observing time map in the detector reference frame for DAMPE pointing to the Vela pulsar in the first year of operation.

gamma-ray source then can be modeled by

$$F(E,\hat{p};\boldsymbol{\lambda}) = S(E;\boldsymbol{\lambda})M(\hat{p})\ . \tag{10}$$

Here $M(\hat{p})$ is a normalized function describing the spatial morphology of the source. For the point source, the spatial distribution can be described with a Dirac delta function, $M(\hat{p}) = \delta(\hat{p} - \hat{p}_0)$, where $\hat{p}_0$ is the direction of the point source. The $S(E;\boldsymbol{\lambda})$ in Equation (10) is the spectrum of the source with its parameters $\boldsymbol{\lambda}$.

To remove the θ dependence of the PSF and energy dispersion, we calculate the exposure-weighted PSF and energy dispersion for any sources included in the analysis

$$\overline{P}(\delta v; E) = \frac{\sum_s \int P(\delta v; E,\theta,s) A_{\rm eff}(E,\theta,\phi,s) t_{\rm obs}(\theta,\phi) {\rm d}\Omega}{\sum_s \int A_{\rm eff}(E,\theta,\phi,s) t_{\rm obs}(\theta,\phi) {\rm d}\Omega}, \tag{11}$$

$$\overline{D}(E'; E) = \frac{\sum_s \int D(E'; E,\theta,s) A_{\rm eff}(E,\theta,\phi,s) t_{\rm obs}(\theta,\phi) {\rm d}\Omega}{\sum_s \int A_{\rm eff}(E,\theta,\phi,s) t_{\rm obs}(\theta,\phi) {\rm d}\Omega}. \tag{12}$$

Considering the excellent energy resolution of DAMPE (i.e., $\sim$ 5 % at 1 GeV and $\sim$ 1 % at 100 GeV (Chang et al. 2017)), the influence of energy dispersion can

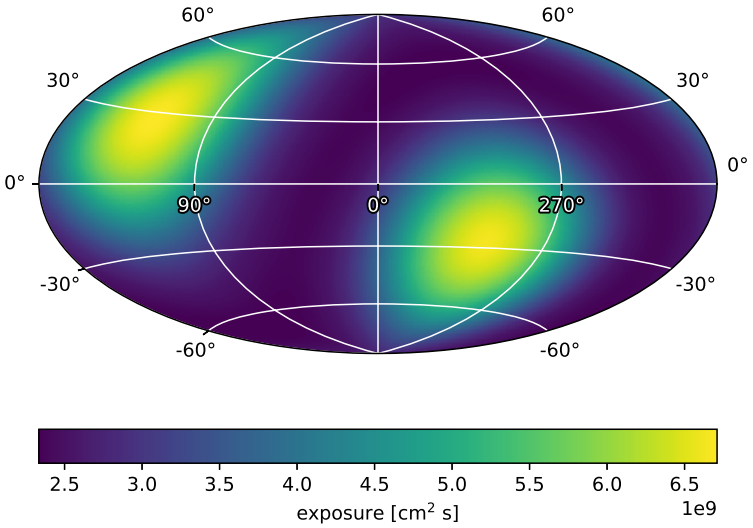

Fig. 7 The exposure map of DAMPE at 10 GeV in the first year shown in a Hammer-Aitoff projection in Galactic coordinates. The maximum value is at the two poles of the equatorial coordinates, while the minimum value is at the equator.

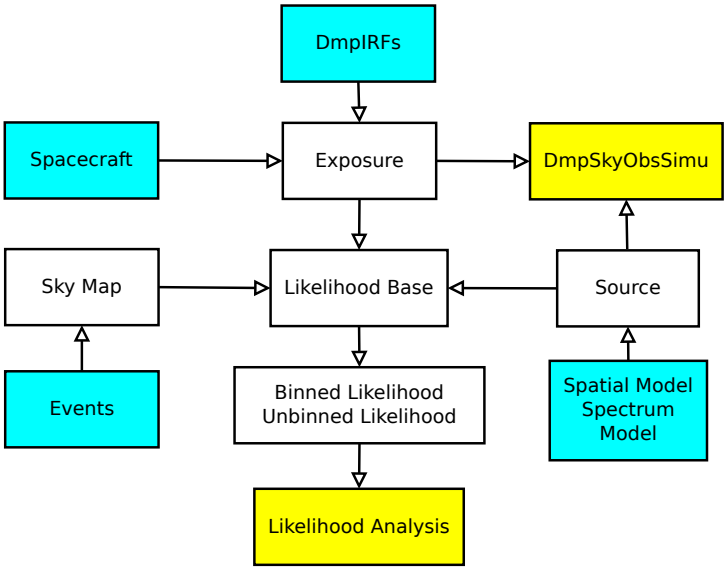

Fig. 8 The structure of DmpST. *Cyan*, *white* and *yellow* represent the input, process and output modules, respectively.

be ignored for most gamma-ray science analysis. The only exception is the case of searching for a narrow-line feature in the gamma-ray spectrum (Ackermann et al. 2015; Liang et al. 2016; Li et al. 2018), which will be performed with other dedicated code. So in the DmpST, we ignore the energy dispersion and regard the measured energy as the true photon energy in the current version; it will be considered in the future if statistics allow.

With the parameterized source model, exposure and exposure-weighted PSF, we can calculate the model-predicted photon rate in bin i (centered on $E_i, \hat{p}'_i$) from the source j

$$r_{ij}(E_i, \hat{p}'_i; \boldsymbol{\lambda}_j) = \int \mathrm{d}\Omega F_{ij}(E_i, \hat{p}; \boldsymbol{\lambda}_j) \times \epsilon(E_i, \hat{p}) \bar{P}(\hat{p}'_i; \hat{p}, E_i) \ . \quad (13)$$

The predicted photon rates are compared to the observation data to determine the model parameters. The information we can get from DAMPE observations is the energy (E), direction ($\hat{p}'$) and time of arrival (t) for each photon. We bin the photons in the region-of-interest (ROI) into a counts cube according to their measured energies and directions. For each bin, the photon number N follows a Poisson distribution with unknown mean R: $p(N; R) =$

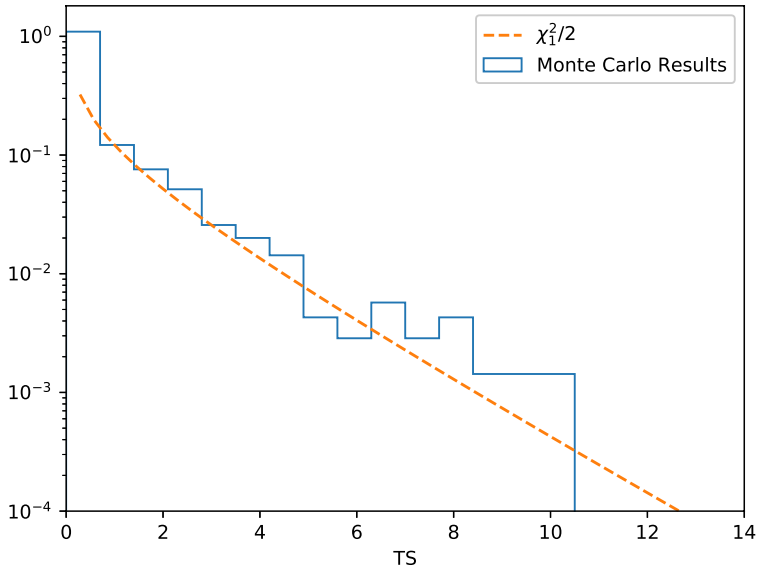

Fig. 9 The *histogram* is the normalized distribution of TS values analyzed from simulated data, and the *dashed line* is the distribution following $\chi^2_1/2$. In the analysis, the null hypothesis is no point source and the alternative hypothesis is the converse.

$R^N/N! \cdot \exp(-R)$. Taking into account all the bins with numbers $\{N_i\}$, the Poisson distribution becomes

$$p(\{N_i\};\{R_i\}) = \prod_{i=1}^{N_{\rm bins}} \frac{R_i^{N_i}}{N_i!} \exp(-R_i)\,. \tag{14}$$

Because of the broad PSF of DAMPE and the strong Galactic diffuse background, the photons in each bin may originate from multiple sources, the parameters of which should be determined simultaneously utilizing likelihood fitting. With the model-predicted photon rates and the real observed data, and based on the Poisson statistics, we construct the binned likelihood function (in logarithm form) by summing over all $N_{\rm bins}$ bins and all $N_{\rm s}$ sources

$$\begin{aligned}\log L(\boldsymbol{\lambda}) &= \sum_{i=1}^{N_{\rm bins}} \left(-\sum_{j=1}^{N_{\rm s}} R_{ij} + N_i \log \sum_{j=1}^{N_{\rm s}} R_{ij} \right) \\ &= \sum_{i=1}^{N_{\rm bins}} \left(-\int {\rm d}t \int {\rm d}E \int {\rm d}\Omega' \sum_{j=1}^{N_{\rm s}} r_{ij}(\boldsymbol{\lambda}_j) \right. \\ &\quad \left. + N_i \log \int {\rm d}t \int {\rm d}E \int {\rm d}\Omega' \sum_{j=1}^{N_{\rm s}} r_{ij}(\boldsymbol{\lambda_j}) \right),\end{aligned} \tag{15}$$

where R_{ij} is the model expected photon number in bin i from source j and the integral is calculated in the corresponding bin i as well.

When the bin widths are taken to be infinitesimal such that there is only 0 or 1 photon in each bin, the summation over $N_{\rm bins}$ bins becomes an integral over the whole energy range and the ROI. Then we get the unbinned form of the likelihood function

$$\begin{aligned}\log L(\boldsymbol{\lambda}) = &- \int {\rm d}t \int {\rm d}E \int_{\rm ROI} {\rm d}\Omega' \sum_{j=1}^{N_{\rm s}} r_j(\boldsymbol{\lambda}_j) \\ &+ \sum_{i=1}^{N_{\rm events}} \log \sum_{j=1}^{N_{\rm s}} r_j(\boldsymbol{\lambda}_j)\,.\end{aligned} \tag{16}$$

By maximizing the likelihood function of (15) or (16), we can calculate the best-fit values of all the free parameters in the source models.

5 IMPLEMENTATION

The code is written with Python, based on the NumPy (van der Walt et al. 2011), SciPy [2], AstroPy (Robitaille et al. 2013) and iminuit (James & Roos 1984) packages. The structure of DmpST is shown in Figure 8.

The input modules are `Events`, `SpaceCraft`, `DmpIRFs`, `Spatial Model`, `Spectrum` and `Model` (shown in cyan in Fig. 8). The `Events` module stores information on photons that are selected from all the events detected by DAMPE using the photon selection algorithm (Xu et al. 2018). The information on a photon includes the time of arrival (t), reconstructed energy (E), reconstructed direction in celestial coordinates (α_{2000}, δ_{2000}, l, b) and in the detector reference frame (θ, ϕ), and trigger type (s). The photons of interest in the analysis can be selected according to their times, energies or directions utilizing the `Events` module and can be binned into a counts map or

[2] `http://www.scipy.org`

a counts cube which is managed by the `Sky Map` module. The `SpaceCraft` module stores the position, direction and live time of DAMPE along with time, and can be used to calculate the observing time of DAMPE for any direction in the sky (see Sect. 3). The `DmpIRFs` module is used to manage information on IRFs, including the effective area matrix, and the parameters of PSF and energy dispersion function. With these parameters and the fitting functions described in Section 2, the distributions of the PSF and energy dispersion can be reconstructed. The `Spatial Model` and `Spectrum` modules provide different kinds of spatial and spectral models of gamma-ray sources, respectively. The `Model` module includes all the models of sources that will contribute photons to the ROI.

The process modules comprise `Sky Map`, `Exposure`, `Source`, `Likelihood Base`, `Binned Likelihood` and `Unbinned Likelihood` (white parts in Fig. 8). The `Sky Map` module manages the information on counts map or counts cube from the `Events` module, such as the photon number and celestial coordinates of each bin. The `Exposure` module calculates the observing time, exposure and exposure-weighted PSF and energy dispersion based on information in the `SpaceCraft` and `DmpIRFs` modules. The `Source` module combines spatial and spectral models based on the `Spatial Model` and `Spectrum` modules for each source in the `Model` module. The `Likelihood Base` module convolves the PSF with the spatial model, and integrates the spectrum over the energy to calculate the expected photon numbers for each source based on the `Sky Map`, `Exposure` and `Source` modules. The `Binned/Unbinned Likelihood` modules construct the likelihood function described in Section 4.

Finally, the `Likelihood Analysis` module implements the maximum likelihood estimation with the Minuit algorithm and the basic outputs are the best-fit values ($\hat{\boldsymbol{\lambda}}$) of source parameters, source fluxes and corresponding statistical uncertainties. Also, we can obtain the confidence level for each source defined as

$$TS_j = -2(\log L(\hat{\boldsymbol{\lambda}}_{0,j}) - \log L(\hat{\boldsymbol{\lambda}}))\,, \tag{17}$$

where $\hat{\boldsymbol{\lambda}}_{0,j}$ is the best-fit parameters without source j included in the model. The TS_j follows a χ^2 distribution with $h - m$ degrees of freedom (Wilks 1938), where h and m are the number of free parameters in the model with/out source j. The `DmpSkyObsSimu` module simulates photons observed by DAMPE with the `DmpIRFs`, `SpaceCraft` and `Source` modules.

The MC simulation was done with the `DmpSkyObsSimu` module with Galactic diffuse emission and isotropic emission included. With the `Likelihood Analysis` module, we analyze the simulated data to confirm the distribution of TS. The null hypothesis is that there is no point source, only the background including Galactic diffuse emission and isotropic emission. The alternative hypothesis is the converse: there is a point source with a power-law spectrum with free normalization parameter. For most point source analyses of DAMPE, the radius of the ROI is $\approx 2 \times S_{\rm p}$ and the typical number of photons N in the ROI is about 25. Figure 9 shows that for $TS > 0$, the distribution of TS follows $\chi^2_1/2$, and one half of the simulations have $TS = 0$ (Mattox et al. 1996).

6 SUMMARY

The GeV gamma-ray sky is an important observation target for DAMPE. To facilitate analyzing the DAMPE gamma-ray data, we have developed a dedicated software named DmpST, which implements maximum likelihood analysis to extract the parameters of sources that contribute to the observed gamma-rays. The DAMPE IRFs that are essential to the gamma-ray data analysis, including the effective area, PSF and energy dispersion, are also derived based on statistics from simulation data. Applying the DmpIRFs and DmpST that are detailed in this paper, scientific analyses of the gamma-ray data could be carried out to obtain the best-fit spectral parameters, fluxes and corresponding statistical uncertainties, and further the spectral energy distribution and light curve of the gamma-ray sources, promoting our understanding of the nature of high energy gamma-ray phenomena.

Acknowledgements This work is supported in part by the National Key Program for Research and Development (2016YFA0400200), the Strategic Priority Research Program of Chinese Academy of Sciences (XDB23040000), the 13th Five-year Informatization Plan of Chinese Academy of Sciences (XXH13506), the National Natural Science Foundation of China (Nos. U1631111, U1738123, U1738136 and U1738210), Youth Innovation Promotion Association of Chinese Academy of Sciences and the Young Elite Scientists Sponsorship Program. In Europe, the activities and data analysis are supported by the Swiss National Science Foundation (SNSF), Switzerland and the National Institute for Nuclear Physics (INFN), Italy.

References

Ackermann, M., Ajello, M., Albert, A., et al. 2012, ApJS, 203, 4
Ackermann, M., et al. 2015, Phys. Rev. D, 91, 122002

Ambrosi, G., An, Q., Asfandiyarov, R., et al. 2019, Astroparticle Physics, 106, 18

Chang, J. 2014, Spac. Sci., 34, 550, *www.cjss.ac.cn/EN/abstract/abstract2067.shtml*

Chang, J., Ambrosi, G., An, Q., et al. 2017, AstroPart. Phys., 95, 6

Ding, M., Zhang, Y., Zhang, Y.-J., et al. 2019, RAA (Research in Astronomy and Astrophysics), 19, 047

James, F., & Roos, M. 1984, Comput. Phys. Commun., 35

Jiang, W., Li, X., Duan, K.-K., et al. 2019, submitted to RAA (Research in Astronomy and Astrophysics)

Kirsch, M. G. F., Altieri, B., Chen, B., et al. 2004, in Proc. SPIE, 5488, UV and Gamma-Ray Space Telescope Systems, eds. G. Hasinger, & M. J. L. Turner, 103

Li, S., Liang, Y.-F., Xia, Z.-Q., et al. 2018, Phys. Rev. D, 97, 083007

Liang, Y.-F., Shen, Z.-Q., Li, X., et al. 2016, Phys. Rev. D, 93, 103525

Ma, P.-X., et al. 2018, arXiv:1808.05720

Mattox, J. R., Bertsch, D. L., Chiang, J., et al. 1996, ApJ, 461, 396

Read, A. M., Rosen, S. R., Saxton, R. D., & Ramirez, J. 2011, A&A, 534, A34

Robitaille, T. P., Tollerud, E. J., Greenfield, P., et al. 2013, A&A, 558, A33

van der Walt, S., Colbert, S. C., & Varoquaux, G. 2011, Computing in Science & Engineering, 13, 22

Wilks, S. S. 1938, Ann. Math. Statist., 9, 60, *https://www.projecteuclid.org/euclid.aoms/1177732360*

Xu, Z.-L., Duan, K.-K., Shen, Z.-Q., et al. 2018, RAA (Research in Astronomy and Astrophysics), 18, 027